Compact diode pumped solid state laser with intracavity pump-enhanced DFG emitting at ~3.5 microns

Liam Gerrit Keith Flannigan * , Ali Atwi , Tyler Kashak , Daniel Poitras , Chang-qing Xu

Posted Date: 2 October 2023

doi: 10.20944/preprints202309.2172.v1

Keywords: nonlinear optics; difference frequency generation; mid-infrared laser; DPSS laser; linear cavity

Article

Compact Diode Pumped Solid State Laser with Intracavity Pump-Enhanced DFG Emitting at ~3.5 Microns

Liam Flannigan [1,*], Ali Atwi [1], Tyler Kashak [1], Daniel Poitras [2] and Chang-qing Xu [1]

[1] Department of Engineering Physics, McMaster University, Hamilton, Ontario L8S 4L8, Canada
[2] Advanced Electronics and Photonics Research Center, National Research Council Canada, Ottawa, Ontario K1A 0R6
* Correspondence: flannilg@mcmaster.ca;

Abstract: We report a diode pumped solid state (DPSS) laser used for intracavity pump-enhanced difference frequency generation (DFG) to create a 3.5 micron laser. Using a 50 mm-long periodically poled lithium niobate (PPLN) crystal inside the cavity of an Nd:YVO_4 solid state laser at 1064 nm with 4.5 W pump power at 808 nm, and a 310 mW C-band signal at 1529 nm, up to 31 mW of mid-infrared output power at 3499 nm is obtained. The cavity requires no active stabilization and/or locking, and the entire cavity is <8 cm in length. The obtained output power corresponds to a black box efficiency of 2.20 $\%W^{-1}$, which is the highest value reported to date for continuous wave DFG based on a bulk nonlinear optical crystal with no active stabilization. Potential future applications in free space optical communication are discussed as well.

Keywords: nonlinear optics; difference frequency generation; mid-infrared laser; DPSS laser; linear cavity;

1. Introduction

Free space optical communication has seen a surge in interest, both for terrestrial first and last mile solutions, as well as optical satellite communication [1,2]. Current efforts have focused on utilizing the short-wave infrared (SWIR) atmospheric transmission window, containing the 1530-1565 nm C-band used in telecommunications. Successful demonstrations utilizing these wavelengths include the SOLISS terminal bidirectional link between the International Space Station (ISS) and an optical ground station at the National Institute of Information and Communications Technology (NICT) in 2019, as well as an inter-satellite demonstration between the CubeSOTA and ETS9-HICALI satellites in 2019 [3,4]. However, SWIR communication suffers significantly from scintillation, scattering, and weather effects. The 3-5 **µm** mid-infrared (MWIR) atmospheric transmission window should offer improved signal to noise ratio and resistance to these adverse effects and could lead to higher link availability and reliability [5,6]. A previous review from our research group expanded on the benefits of the MWIR band and identified cascade lasers, as well as difference frequency generation (DFG) using nonlinear optical crystals, as the most promising lasers for use in MWIR transmitters [7–9]. Cascade lasers offer large modulation bandwidths and can cover the entire MWIR spectrum, but typically operate between 77-250 K, which is inconvenient for many applications [10,11]. DFG offers room temperature operation and large modulation bandwidths, with potential to achieve up to watt-level continuous wave output power [12]. Typically, OPOs are used due to their resonant structure offering high output powers and tunable output wavelengths. However, the use of DFG allows us to inject a C-band signal beam, offering multi-gigabit per second modulation speeds, which can be faster than directly modulating the OPO pump beam [8]. In this paper, we aim to address the lack of high efficiency intracavity MWIR lasers by presenting a novel DFG laser that uses a simplified linear cavity to reduce the size and sensitivity to alignment, and to achieve high efficiency. The laser is stable while free running with no need for external cavity stabilization or locking. In the cavity, only the pump is resonant, as the signal is coupled into the cavity and the idler

Preprints (www.preprints.org) | NOT PEER-REVIEWED | Posted: 2 October 2023 doi:10.20944/preprints202309.2172.v1

is coupled out of the cavity in a single pass. We see this as the first step to demonstrating a viable high-power mid-infrared source capable of high-speed modulation.

A common metric used to evaluate DFG frequency converters is DFG efficiency, presented according to the formula in Equation (1):

$$\eta_{DFG} = 100\% \times \frac{P_{DFG}}{P_{pump}P_{signal}}, \quad (1)$$

With the efficiency expressed in units of $\%\mathbf{W^{-1}}$. Here, $\boldsymbol{P_{DFG}}$ is the output DFG power, $\boldsymbol{P_{pump}}$ is the input pump power directly before the nonlinear crystal, and $\boldsymbol{P_{signal}}$ is the input signal power directly before the nonlinear crystal. However, this approach does not consider the efficiencies and coupling losses of the pump and signal sources, which can be important in power limited scenarios where maximizing efficiency is key. So, from a practical application point of view, an interesting metric to compare the efficiency of various DFG structures is the black box efficiency with units of $\%\mathbf{W^{-1}}$, presented here as Equation (2):

$$\eta_{BB} = 100\% \times \frac{\eta_{signal}\eta_{pump}P_{DFG}}{P_{pump}P_{signal}}, \quad (2)$$

where $\boldsymbol{\eta_{pump}}$ is the diode pumping efficiency for the fiber pump source and $\boldsymbol{\eta_{signal}}$ is the diode pumping efficiency of the fiber signal source, assuming fiber lasers are used as pump and signal sources. We mention fiber pump and signal sources specifically as these are commonly used for pumping both DFG and OPO structures. Many of the presented structures in the following section make use of 1064 nm Yb-doped fiber lasers (pumped by 9xx nm diode laser) as pump sources. These have optical-to-optical efficiencies of ~60%, so a value of $\boldsymbol{\eta_{pump} = 0.6}$ was assumed for these fiber lasers [13]. For devices using direct 1064 nm diode pumping, there is no additional optical conversion step, and so a value of $\boldsymbol{\eta_{pump} = 1}$ can be used. For the signal fiber, erbium doped fiber amplifiers (EDFAs) are often used. Unfortunately, it is harder to find a standard operating efficiency for the pump diodes in EDFAs, and most authors only include the output power from the EDFA ($\boldsymbol{P_{signal}}$). Thus, we've assumed $\boldsymbol{\eta_{signal} = 1}$ for all EDFAs so that they can be easily compared. This does increase the overall efficiency reported in this paper, so we mention this to avoid claims of inflating the efficiency values intentionally. While we do not claim that our device has the highest DFG efficiency reported, we do claim that it has the highest black box efficiency of the bulk crystal, free-running DFG devices we've reviewed.

We performed a literature review of state-of-the-art single pass and intracavity mid-infrared bulk DFG devices. In 2020, Guha et al. reported a single pass DFG configuration, emitting 3.55 W at 3400 nm with 43.3 W 1064 nm via fiber laser pump and 31 W 1550 nm signal via EDFA, corresponding to a DFG efficiency of 0.264 $\%\mathbf{W^{-1}}$ and a black box efficiency of $0.\mathbf{159}\ \%\mathbf{W^{-1}}$ [14]. In 2019, Huang et al. demonstrated 60 mW of DFG power at 3393 nm for 1 W of 1064 nm fiber laser pump and 1 W of 1550 nm, corresponding to a DFG efficiency of 5.8 $\%\mathbf{W^{-1}}$ and a black box efficiency of 2.43 $\%\mathbf{W^{-1}}$, which accounts for the additional loss of the wavelength division multiplexer used [15]. Huang et al's cavity is also actively stabilized via dither-locking. These devices represent the highest efficiency single pass and intracavity efficiencies we found, respectively, but other devices were reviewed with efficiencies in the same order of magnitude [16–20]. These works serve as a representative sample of the state-of-the-art for bulk crystals. Additionally, waveguides allow for tight confinement of the pump and signal beams over the entire length of the nonlinear medium, which boosts efficiency versus bulk crystals. For example, the highest efficiency mid-infrared waveguide nonlinear frequency converter we found has an internal DFG efficiency of 100 $\%\mathbf{W^{-1}}$ and a black box efficiency of 60 $\%\mathbf{W^{-1}}$ [21]. However, the reported coupling losses are ~-17 dB for both the pump and signal, which would lower the black box efficiency to less than 1 %/W. Hu et al. demonstrated a high-efficiency coupler that could reduce losses for similar thin-film lithium niobate devices to -0.5 dB [22]. Should this low insertion loss be coupled with a high efficiency waveguide device, it would have much higher efficiency than the bulk crystal devices reviewed above [23,24]. For now, the main niche for bulk devices is relative cost, ease of manufacturing, and ease of use. Nonlinear waveguide properties are critically dependent on their fabrication quality, as even small imperfections can

Preprints (www.preprints.org) | NOT PEER-REVIEWED | Posted: 2 October 2023 doi:10.20944/preprints202309.2172.v1

degrade final performance [25]. So, in the short term, bulk crystals remain easy to source off the shelf with a high level of quality, and linear cavities like the one presented in this manuscript are easy to set up and align. However, as manufacturing continues to improve, waveguide-based mid-infrared sources will be preferable to bulk crystals for many applications. As such, we want to make it clear we limit the novelty claim for our device to bulk crystal devices.

In this work, we implement a hemispherical cavity using Nd:YVO_4 as a gain medium to produce a 1064 nm pump. The resonator contains a periodically poled lithium niobate (PPLN) nonlinear crystal, as well as a dichroic mirror that couples an amplified tunable C-band laser into the cavity. We obtained a black box efficiency of 2.20 $\%\mathbf{W^{-1}}$, emitting at 3499 nm with 4.5 W 808 nm pump and 310 mW of 1529 nm signal. This device offers the highest black box efficiency for bulk nonlinear crystal frequency converters in a linear cavity without the use of active cavity stabilization. Additionally, our modelling work shows good agreement with experimental results. What follows is a detailed examination of the experimental set-up and a brief review of the theoretical modelling work.

2. Materials and Methods

A schematic diagram of the experimental setup is depicted in Figure 1. It consists of a diode-pumped solid-state (DPSS) laser resonator (Nd:YVO_4, Dientech) with a PPLN nonlinear crystal inserted into the cavity. The hemispherical resonator was intentionally selected as it allows for a compact cavity set up and is easy to align. Additionally, this linear cavity requires no active stabilization as we've demonstrated experimentally. This reduces complexity and costs without the need for piezoelectric transducers or lock-in amplifiers to facilitate long-term cavity stability. The following cavity parameters were designed with the help of *reZonator*, an open-source cavity modelling software capable of modelling arbitrary optical systems [26]. The reZonator model is summarized in Figure 1 below:

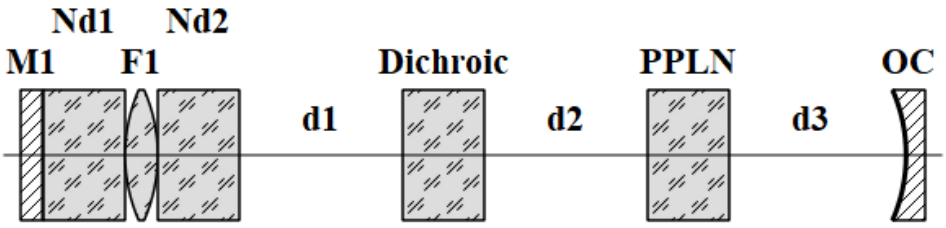

Figure 1. Simplified cavity layout as modelled in reZonator. Note that the components are not to scale.

In this model, M1 represents the HR coating at 1064 on the Nd:YVO_4. The 5 mm gain medium has been split into two 2.5 mm slabs with refractive index n = 2.16 and a thin lens in the middle, in order to approximate the thermal lens as well. The thermal lens focal length was determined to be ~50 mm, which matched the output beam parameters and output power well, and lines up with similar experimental data [27]. Distances d1, d2, and d3 are 5 mm, 10 mm, and 5 mm, respectively. The dichroic is a 1.8 mm slab with refractive index n = 1.5, while the PPLN is 50 mm with a refractive index of n = 2.2. The OC has a radius of curvature of 100 mm. This results in a 1064 nm pump beam radius in the middle of the PPLN of ~100 µm, which will be used as an input to the nonlinear simulation later.

An 808 nm 125 **µm** core diameter multimode fiber pigtailed diode laser (AeroDIODE 808LD-2-0-0) emitting up to 4.5 W optical power was imaged onto the Nd:YVO_4 gain medium using a GRIN lens (Edmund Optics #64-544). The Nd:YVO_4 gain medium was HR coated at 1064 nm (R>99.9%) and high transmission (HT) coated at 808 nm (T>95%) at the input facet, and anti-reflection (AR) coated at 1064 nm (T>99.8%) at the output facet. This was followed by a dichroic mirror (Custom unit fabricated at National Research Council) with a transmission of 99.3% at 1064 nm and a reflectivity of 70% at 1529 nm, both at an angle of incidence of 45°, for s-polarized light. A 50 mm-long 5mol%

Preprints (www.preprints.org) | NOT PEER-REVIEWED | Posted: 2 October 2023 doi:10.20944/preprints202309.2172.v1

MgO doped PPLN crystal (Custom from HCPhotonics) with a period of 30.3 µm was mounted to a copper heat sink with a thermoelectric cooler that can be controlled to within 0.05 °C. The input facet of the PPLN was AR coated for 1064 nm and 1529 nm (T>99.7%) and the output facet was AR coated for 1064 nm (T>99.7%) and 3.5 µm (T>95%). The output coupler (OC) was a CaF_2 plano-concave mirror (Custom from Fuzhou Witoptics) with radius of curvature of 100 mm, HR coated for 1064 nm (R=99.85%) and AR coated for ~3.5 µm (T=92%). A 50 mm focal length AR coated CaF plano-convex lens (Thorlabs LA5183-E) was placed after the OC to collimate the divergent 3499 nm light. A thermal power sensor (Thorlabs S401C) was used to measure the DFG power after filtering out the pump and signal with a Germanium (Ge) filter (Thorlabs WH91050-C9). The dichroic mirror was used to couple in a tunable C-band laser (Agilent 8164B) at 1529 nm, which was amplified via a polarization-maintained EDFA (CiviLaser EDFA-C-BA-26-PM). To increase the working distance of the C-band laser, the collimated EDFA output was passed through a 5x beam expander (Thorlabs GBE05-C) followed by a 100 mm focal length plano-convex lens (Thorlabs LA1050-C) to focus the laser into the center of the PPLN. This design was simulated in Zemax which predicted a beam waist radius of 55 µm in the center of the PPLN, ensuring that the confocal focusing criterion was met. This was required due to space limitations on the optical bench.

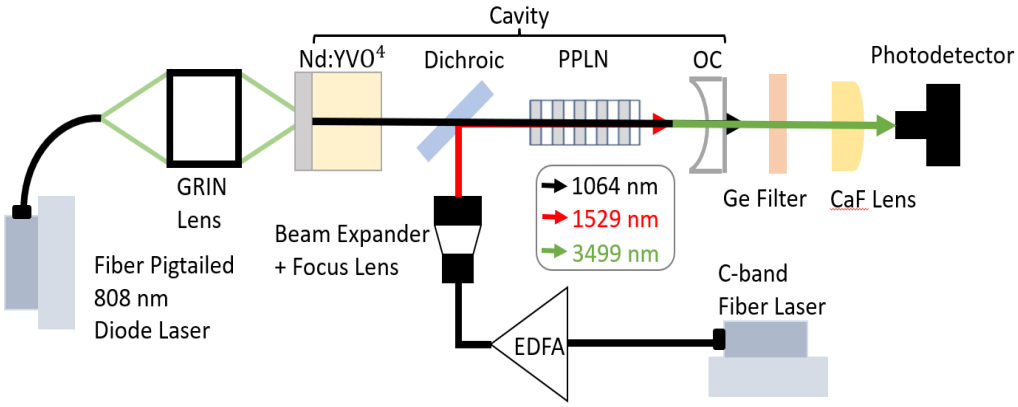

Figure 2. Experimental schematic diagram of the intracavity DFG laser. The fibers for the C-band laser and EDFA are polarization maintaining and single mode, and the total cavity length is <8 cm.

A scanning slit beam profiler (Thorlabs BP209IR1) was used to verify the beam diameters. For the C-band laser, the beam profiler was placed at the focus after the beam expander assembly. The distance from the beam profiler and the beam waist matched a Zemax simulation well, with a waist diameter of 110 µm at 10.5 cm from the assembly output. The cavity waist was confirmed by taking several measurements of the gaussian beam diameter outside of the cavity, and then deriving the gaussian waist using the experimental data. The measured waist diameter of 200 µm was close to the predicted value of 190 µm.

We also describe the simulation work presented in the results section. This is a significantly modified version of work our group has presented previously, although adapted for DFG as opposed to SHG [28]. A flowchart summarizing the flow of the simulation step by step is presented in Figure 3.

Preprints (www.preprints.org) | NOT PEER-REVIEWED | Posted: 2 October 2023 doi:10.20944/preprints202309.2172.v1

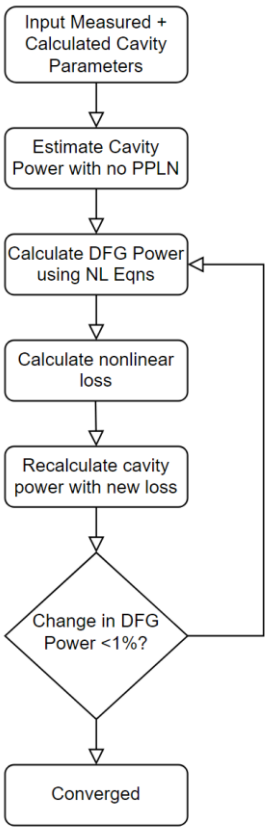

Figure 3. A flowchart summarizing the modelling work. Input parameters are experimentally measured where possible, otherwise they are simulated, or use known values from literature.

To start, we must estimate the incident pump and signal power incident on the nonlinear medium. The signal power is measured experimentally before it is coupled into the cavity, while estimating the intracavity 1064 nm pump power is more involved. A spatially dependent rate equation model was used to derive the intracavity 1064 nm power as detailed by Risk and summarized below in Equation (3): [29]

$$F = \frac{1+\frac{B}{fS}\ln(1+fS)}{f\int_0^{\infty}\frac{\exp[-(a^2+1)x]}{1+fS\exp(-a^2x)}}, \tag{3}$$

Where $\boldsymbol{a = \omega_P/\omega_L}$ is the ratio of the 808 nm pump and 1064 nm laser beam waists, f is the total Boltzmann factor of the gain medium, $\boldsymbol{B = \frac{2N_1^0\sigma l}{L+T}}$ is the ratio of reabsorption loss to fixed cavity loss with L being the total cavity loss, T is the transmission loss from the output coupler, $\boldsymbol{\sigma}$ is the emission cross section of the gain medium, $\boldsymbol{l}$ is the length of the gain medium, and $\boldsymbol{N_1^0}$ is the doping concentration of the Nd in the gain medium. F is a normalized variable proportional to pump power, and S is a normalized variable proportional to internal laser power. Then, by solving for dS/dF, we can derive the pump threshold and slope efficiency in terms of S and F and convert them to real pump power and output laser power as follows.

Once dS/dF has been found numerically, the external slope efficiency of the laser can be found using Equation (4):

$$\frac{dP_{out}}{dP_P} = \frac{T}{L+T}\frac{v_L}{v_P}\eta_a\frac{dS}{dF}, \tag{4}$$

Where $\boldsymbol{vL/vP}$ is the ratio of frequencies of the lasing and pump light, also known as the quantum defect. $\boldsymbol{\eta_a}$ is the absorption efficiency of the incident pump photons in the gain medium, and the ratio $\boldsymbol{\frac{T}{L+T}}$ is the ratio of laser photons exiting the cavity via the output coupling mirror. We

Preprints (www.preprints.org) | NOT PEER-REVIEWED | Posted: 2 October 2023 doi:10.20944/preprints202309.2172.v1

can then solve for the pump threshold of the laser to fully define the expected output power vs pump power curve, as shown in Equations (5) and (6) below:

$$P_{P,th} = \frac{\pi h v_p (\omega_L^2 + \omega_P^2)(L + T + 2\sigma N_1^0 l)}{4\sigma\tau\eta_a f} \quad (5)$$

$$F_{th} = \frac{(1 + a^2)(1 + B)}{f}, \quad (6)$$

Where $\boldsymbol{\tau}$ is the upper manifold lifetime of the gain medium and h is the Planck's constant. Finally, we convert F to $\boldsymbol{P_P}$ by $\boldsymbol{P_P} = \left(\frac{P_{th}}{F_{th}}\right)\boldsymbol{F}$, and we use the derived slope efficiency to determine the expected output power from the laser from the threshold onwards. Then, since the output coupler reflectivity is well known, this allows us to estimate the circulating power within the cavity as well. This determines the input power to the nonlinear medium for the following step of the modelling work.

After determining the input pump and signal power, we use the nonlinear wave equations for DFG to estimate the output idler power as shown in equations (7) and (8) [30]:

$$\frac{dA_1}{dz} = \frac{2id_{eff}\omega_1^2}{k_1 c^2} A_3 A_2^* e^{i\Delta kz} \quad (7)$$

$$\boldsymbol{\frac{dA_2}{dz} = \frac{2id_{eff}\omega_2^2}{k_2 c^2} A_3 A_1^* e^{i\Delta kz}} \quad (8)$$

Where A1 represents the signal wave, A2 represents the idler wave, and A3 represents the pump wave. In this form, we have assumed that the cavity pump power is strong and effectively constant, as the conversion efficiency of the DFG process is low enough that nonlinear losses from conversion are negligible. We still include the nonlinear loss step in Figure 3 as we anticipate the nonlinear loss to become significant in the future once we increase both the pump and signal power, thus increasing the overall efficiency for nonlinear conversion. This increased conversion efficiency acts as an additional source of loss within the cavity, and so must be accounted for to accurately model intracavity frequency conversion at high powers. We temperature tune our PPLN to achieve good phase matching, and the temperature dependence of the PPLN is modelled using the Sellmeier equation for MgO doped PPLN [31]. By using this model, we can accurately predict the output DFG power as a function of input pump power, as well as the temperature dependence of the DFG power via the Sellmeier equation. These results are presented in the following Results section alongside our experimental results, and the two are in good agreement. Future work for expanding the simulation in the future is covered in the Discussion section. Finally, we present our simulation inputs used to generate our results in Table 1 below.

Table 1. Input parameters to the model. Any value measured experimentally or simulated by the authors is designated by "This work". Cited values are from literature.

Parameter	Value	Ref.
Nonlinear coefficient (d_{33})	27 pm/V	[30]
Nd:YVO_4 length (l)	8 mm	This work
Output Coupler Transmission (T) at 1064 nm	0.15%	This work
Round-trip Losses (L)	3%	This work
Absorption efficiency η_a	99%	This work
Boltzmann Factor (f)	0.6	[32]
Upper manifold lifetime (τ)	90 μs	[33]

Preprints (www.preprints.org) | NOT PEER-REVIEWED | Posted: 2 October 2023 doi:10.20944/preprints202309.2172.v1

Lasing beam radius (ω_L)	190 μm	This work
Pump beam radius (ω_P)	250 μm	This work
Pump beam diameter in PPLN	100 μm	This work
Signal beam diameter in PPLN	55 μm	This work
Nd doping	0.5 at. %	This work
PPLN refractive index	~2.2	[31]
Stimulated emission cross section (σ)	$25 \times 10^{-19}\text{cm}^2$	[34]

3. Results

3.1. Output Power Testing

Figure 4 shows the leaking 1064 nm power from the laser cavity as a function of the 808 nm optical pump power. The squares represent the experimental data while the solid line represents the predicted leaking power from the simulation. The leaking 1064 nm power was measured with all components in the resonator and the PPLN temperature tuned to minimize nonlinear losses. The simulation used the measured reflectivity and transmission values for intracavity components to generate a total intracavity loss. The measured and simulated power values are in good agreement, implying that the estimated loss and 1064 nm input power for the DFG simulation is accurate.

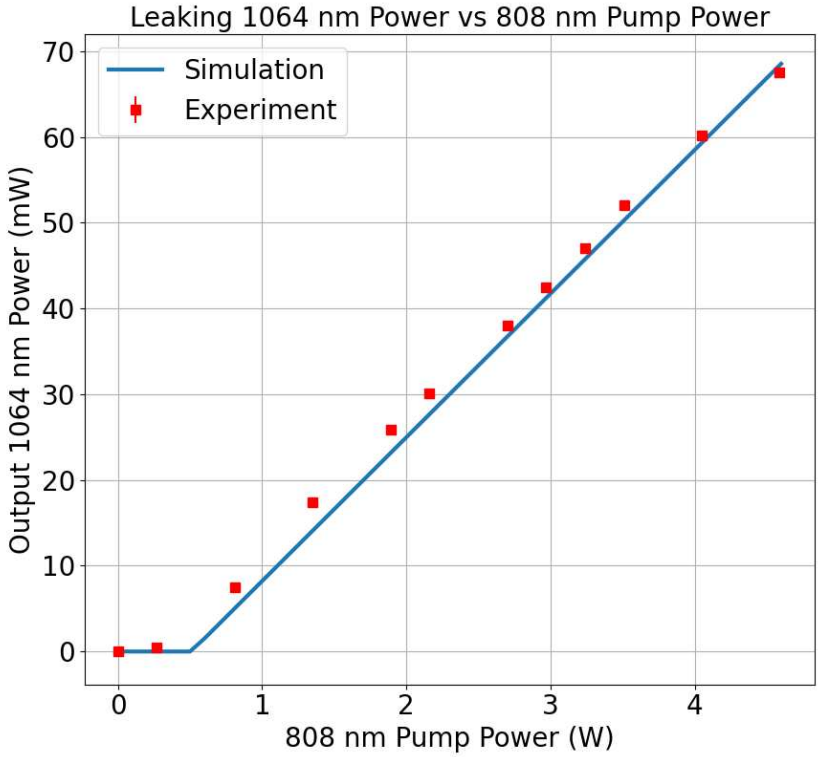

Figure 4. Measured and simulated leaking 1064 nm power vs. 808 nm pump power with all devices in the resonator to account for linear losses. Error bars are present but smaller than the data markers.

After collecting the 1064 nm data, the C-band laser was coupled into the PPLN, and DFG power as high as 31 mW at 3499 nm was obtained at a pump power of 4.5 W 808 nm and a C-band power of 310 mW (measured at the output facet of the C-band collimator). This corresponds to a black box efficiency of 2.20 $\%W^{-1}$. The simulated DFG power is compared to the measured experimental results, as shown in Figure 5. The x-axis is the 808 nm optical pump power, and the y-axis is the DFG output power after the Ge filter. The squares represent experimental data while the solid line is the

Preprints (www.preprints.org) | NOT PEER-REVIEWED | Posted: 2 October 2023 doi:10.20944/preprints202309.2172.v1

simulated DFG power. The simulation assumes that both input beams are focused at the center of the PPLN, and the beam diameters and power values are those measured earlier. The trend is in good agreement, with some outliers in the 2-3 W pump range. This discrepancy could be attributed to non-ideal overlap of the 1064 nm and C-band beams, as the hemispherical cavity prevents strong focusing of the 1064 nm beam at the center of the PPLN, and the thermal lens power will change with pump power as well. Nonetheless, the simulated trend can still be used to predict the order of magnitude experimental DFG performance to a reasonable level of accuracy.

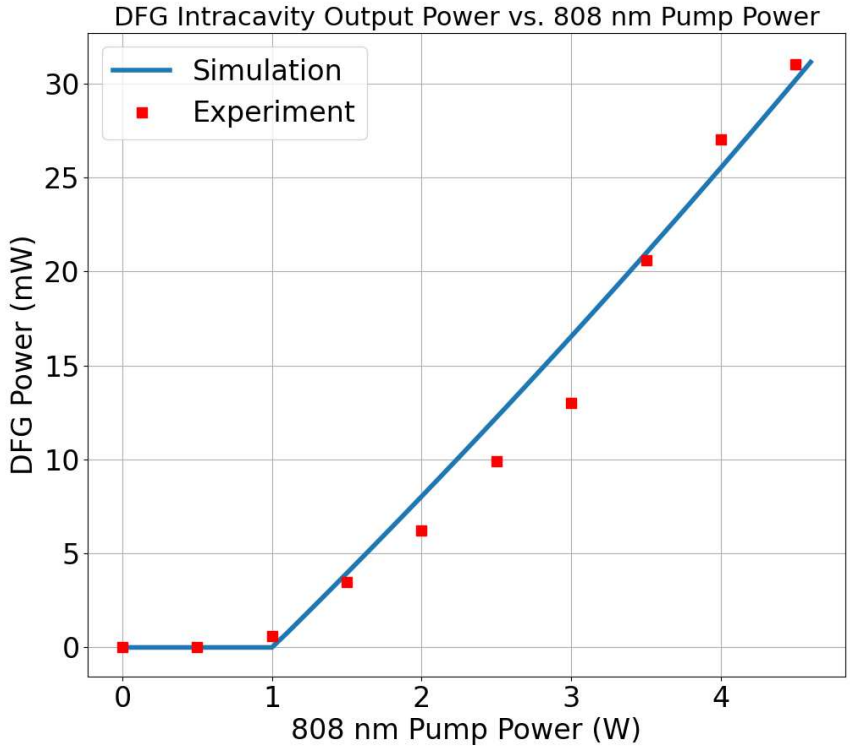

Figure 5. Measured and simulated output DFG power vs 808 nm pump power with all losses accounted for. The simulation data is the solid line.

3.2. Temperature Testing

To study the temperature tolerance of the DFG laser, the temperature tuning curve of the DFG power was measured. We then simulated the temperature dependence of DFG, using the Sellmeier equation for MgO doped lithium niobate [31]. The results are presented in Figure 6. The x-axis is the temperature of the PPLN, and the y-axis is the normalized DFG power. The squares are experimental data, while the solid line is the simulated curve. The good agreement of the peak power location and full width at half maximum (FWHM) confirms the presence of DFG output. The tail on the left side can be attributed to a combination of the tightly focused gaussian signal beam, elliptical focusing, and tilt of the input beams with respect to the optical axis [35]. This was obtained using a standard off-the-shelf thermoelectric cooler, and a machined in-house copper heat sink that also served as the housing for the nonlinear crystal. The FWHM of the main peak is ~6 deg C, demonstrating that the laser can easily be operated at a stable temperature with standard components. If desired, this temperature bandwidth could be increased via chirping of the PPLN at the cost of nonlinear conversion efficiency.

Preprints (www.preprints.org) | NOT PEER-REVIEWED | Posted: 2 October 2023 doi:10.20944/preprints202309.2172.v1

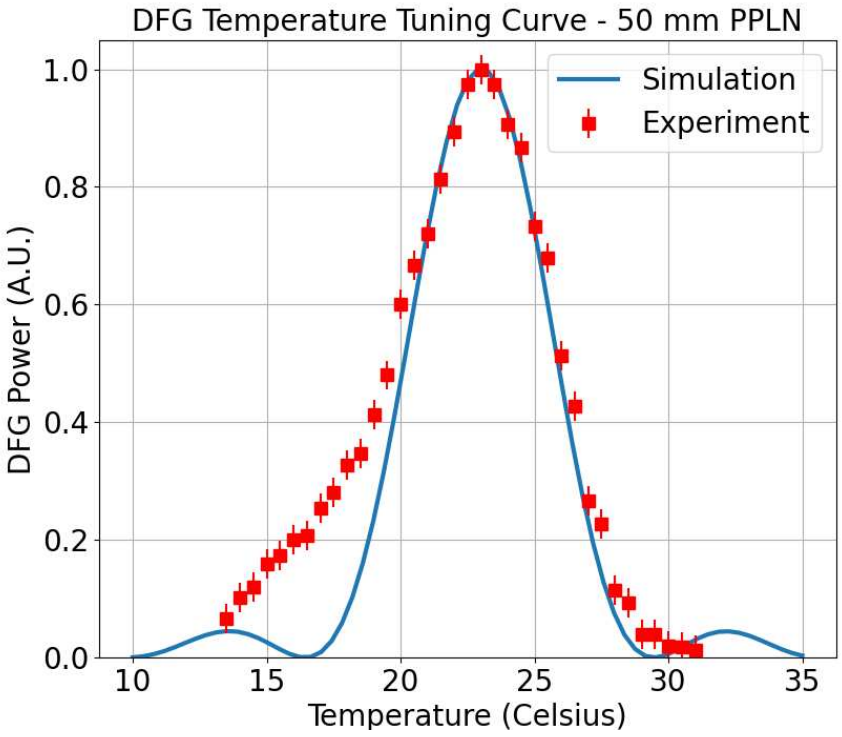

Figure 6. Theoretical temperature tuning curve vs measured experimental data.

4. Discussion

The results are promising, showing that we can easily achieve state-of-the-art black box efficiency with a compact, linear cavity without stabilization. According to our modelling, this represents close to the best-case black box efficiency we can reasonably expect for this design. While it is theoretically possible to improve our efficiency to up to ~2.40-2.50 %/W, this was only achieved by further improving the optical coatings, which are already close to the upper limit of performance. A larger efficiency gain would be possible if the pump beam could be made smaller to better overlap with the 55 **µm** signal beam waist at the center of the PPLN, as there is a noticeable mismatch with the ~100 um pump derived from the cavity simulation. However, this may require a significant cavity redesign, and something other than the hemispherical cavity that we selected due to its simplicity. We will have to investigate in future work whether decreasing the pump beam size is possible, or if increasing the signal beam size is worth the loss in intensity versus the increase in overlap between the pump and signal.

While our model agrees well with the current experimental results, there are several areas where it could be improved to facilitate future work. First, the model does not consider thermal effects outside of the thermal lensing approximated in the cavity simulation. A future test would involve increasing both the pump 808 nm power and the signal C-band power to see if higher output power and black box efficiency can be achieved. However, this will increase the prevalence of thermal lensing in the Nd:YVO4 such that it may affect cavity stability. Additionally, the higher thermal load of a multi-watt level signal coupled with the tens of watts of pump present in the cavity may change the beam properties inside of the nonlinear crystal. Another important factor is the increased nonlinear losses within the cavity at higher efficiencies and pump powers. Currently, the DFG conversion efficiency is low enough that the nonlinear losses are not significant relative to the linear losses within the cavity (scattering, absorption, non-ideal coatings, etc.). Any attempts to increase efficiency will also increase the prevalence of intracavity nonlinear loss. We have previously demonstrated that in a simple nonlinear process like SHG, the nonlinear loss can significantly affect the expected output power and thermal properties of intracavity frequency conversion at higher efficiencies [28]. We have no reason to believe there won't be similar phenomena to observe at higher device powers and higher efficiencies with intracavity DFG as well. These are important points to

consider and investigate in future work, as the efficiency we've reported may not be maintained at higher pump and signal powers as a result.

Future work will focus on adapting the device presented here for free space optical communications. Experiments will include using a 10 W EDFA and 10 W 808 nm pump to push for watt-level DFG power. This is a vital milestone for satellite-to-ground optical communication in low earth orbit, as previous work has identified that 1-2 W CW power is recommended for high link availability and low bit error rates [36]. We will also pursue modulating the C-band source at gigabit speeds, as this opens the door to high-speed weather resistant free space optical links for both last mile applications and longer distance links, due to the combination of high speed and high transmitter power. To the best of our knowledge, a gigabit speed mid-infrared link has not been demonstrated over distances greater than a few kilometers, so we hope to perform a practical demonstration using drones and high-altitude platforms in the coming months as further proof of principle.

5. Conclusions

In conclusion, a compact intracavity DFG MWIR laser with promise for free space communication has been demonstrated. A black box efficiency as high as 2.20 $\%\mathbf{W^{-1}}$ has been achieved with a maximum output power of 31 mW for input pump and signal powers of 4.5 W and 310 mW, respectively. The cavity is under 8 cm in length and could be made more compact with professional packaging. The linear cavity requires no active stabilization, which is also a notable benefit. In future work, we expect that this laser will be capable of watt-level output power and provide what may be the first opportunity for a long-distance free space link in the mid-infrared between either a drone or high-altitude platform.

6. Patents

This work is a developed version of the transmitter device laid out in the patent US20210141282A1 – Mid-infrared wavelength optical transmitter and receiver.

Author Contributions: Conceptualization, Liam Flannigan and Chang-qing Xu; Data curation, Liam Flannigan, Ali Atwi and Tyler Kashak; Formal analysis, Liam Flannigan and Ali Atwi; Funding acquisition, Liam Flannigan and Chang-qing Xu; Investigation, Liam Flannigan, Ali Atwi and Tyler Kashak; Methodology, Liam Flannigan, Ali Atwi, Tyler Kashak, Daniel Poitras and Chang-qing Xu; Project administration, Daniel Poitras and Chang-qing Xu; Resources, Daniel Poitras and Chang-qing Xu; Software, Liam Flannigan; Supervision, Chang-qing Xu; Validation, Liam Flannigan, Ali Atwi, Tyler Kashak and Daniel Poitras; Visualization, Liam Flannigan; Writing – original draft, Liam Flannigan; Writing – review & editing, Liam Flannigan, Ali Atwi, Tyler Kashak, Daniel Poitras and Chang-qing Xu.

Funding: This research was funded by the Natural Sciences and Engineering Research Council of Canada (NSERC) and the High Throughput and Secure Networks Challenge Program at the National Research Council of Canada (NRC).

Data Availability Statement: Data underlying the results presented in this paper may be obtained from the authors upon reasonable request.

Acknowledgments: The authors would like to thank Saju Thomas of MDA (Kanata) and Dr. Atieh of Optiwave Systems Inc. for helpful discussions.

Conflicts of Interest: The authors declare no conflict of interest. The funders had no role in the design of the study; in the collection, analyses, or interpretation of data; in the writing of the manuscript; or in the decision to publish the results.

References

[1] A. Trichili, M. A. Cox, B. S. Ooi, and M.-S. Alouini, "Roadmap to free space optics," *J. Opt. Soc. Am. B, JOSAB*, vol. 37, no. 11, pp. A184–A201, Nov. 2020, doi: 10.1364/JOSAB.399168.

[2] M. M. Abadi, Z. Ghassemlooy, N. Mohan, S. Zvanovec, M. R. Bhatnagar, and R. Hudson, "Implementation and Evaluation of a Gigabit Ethernet FSO Link for 'The Last Metre and Last Mile Access Network,'" in *2019 IEEE International Conference on Communications Workshops (ICC Workshops)*, May 2019, pp. 1–6. doi: 10.1109/ICCW.2019.8757150.

[3] A. Carrasco-Casado *et al.*, "Intersatellite-Link Demonstration Mission between CubeSOTA (LEO CubeSat) and ETS9-HICALI (GEO Satellite)," in *2019 IEEE International Conference on Space Optical Systems and Applications (ICSOS)*, Oct. 2019, pp. 1–5. doi: 10.1109/ICSOS45490.2019.8978975.

[4] K. Iwamoto *et al.*, "Experimental results on in-orbit technology demonstration of SOLISS," in *Free-Space Laser Communications XXXIII*, SPIE, Mar. 2021, pp. 51–57. doi: 10.1117/12.2578089.

[5] E. Leitgeb *et al.*, "Analysis and evaluation of optimum wavelengths for free-space optical transceivers," in *2010 12th International Conference on Transparent Optical Networks*, Jun. 2010, pp. 1–7. doi: 10.1109/ICTON.2010.5549009.

[6] M. A. Khalighi and M. Uysal, "Survey on Free Space Optical Communication: A Communication Theory Perspective," *IEEE Communications Surveys & Tutorials*, vol. 16, no. 4, pp. 2231–2258, 2014, doi: 10.1109/COMST.2014.2329501.

[7] L. Flannigan, L. Yoell, and C. Xu, "Mid-wave and long-wave infrared transmitters and detectors for optical satellite communications—a review," *J. Opt.*, vol. 24, no. 4, p. 043002, Mar. 2022, doi: 10.1088/2040-8986/ac56b6.

[8] N. S. Prasad, "Optical Communications in the mid-wave IR spectral band," in *Free-Space Laser Communications: Principles and Advances*, A. K. Majumdar and J. C. Ricklin, Eds., in Optical and Fiber Communications Reports. , New York, NY: Springer, 2008, pp. 347–391. doi: 10.1007/978-0-387-28677-8_8.

[9] F. Grillot *et al.*, "Recent advances in high-speed data communications using mid-infrared quantum cascade lasers," in *Novel In-Plane Semiconductor Lasers XXII*, SPIE, Mar. 2023, pp. 97–102. doi: 10.1117/12.2651132.

[10] B. Hinkov, A. Hugi, M. Beck, and J. Faist, "Rf-modulation of mid-infrared distributed feedback quantum cascade lasers," *Opt. Express, OE*, vol. 24, no. 4, pp. 3294–3312, Feb. 2016, doi: 10.1364/OE.24.003294.

[11] A. Calvar *et al.*, "High frequency modulation of mid-infrared quantum cascade lasers embedded into microstrip line," *Applied Physics Letters*, vol. 102, no. 18, p. 181114, May 2013, doi: 10.1063/1.4804370.

[12] C. Xi, P. Wang, X. Li, and Z. Liu, "Highly efficient continuous-wave mid-infrared generation based on intracavity difference frequency mixing," *High Power Laser Science and Engineering*, vol. 7, p. e67, Jan. 2019, doi: 10.1017/hpl.2019.45.

[13] S. Unger, A. Schwuchow, S. Jetschke, V. Reichel, A. Scheffel, and J. Kirchhof, "Optical properties of Yb-doped laser fibers in dependence on codopants and preparation conditions," in *Optical Components and Materials V*, SPIE, Feb. 2008, pp. 270–280. doi: 10.1117/12.762967.

[14] S. Guha, J. O. Barnes, and L. P. Gonzalez, "Multiwatt-level continuous-wave midwave infrared generation using difference frequency mixing in periodically poled MgO-doped lithium niobate," *Opt. Lett., OL*, vol. 39, no. 17, pp. 5018–5021, Sep. 2014, doi: 10.1364/OL.39.005018.

[15] K. Huang *et al.*, "Observation of spectral mode splitting in a pump-enhanced ring cavity for mid-infrared generation," *Opt. Express, OE*, vol. 27, no. 8, pp. 11766–11775, Apr. 2019, doi: 10.1364/OE.27.011766.

[16] Q. Hao *et al.*, "Mid-infrared transmitter and receiver modules for free-space optical communication," *Appl. Opt., AO*, vol. 56, no. 8, pp. 2260–2264, Mar. 2017, doi: 10.1364/AO.56.002260.

[17] Y. Su *et al.*, "10 Gbps DPSK transmission over free-space link in the mid-infrared," *Opt. Express, OE*, vol. 26, no. 26, pp. 34515–34528, Dec. 2018, doi: 10.1364/OE.26.034515.

[18] A. C. Gray, S. A. Berry, L. G. Carpenter, J. C. Gates, C. B. E. Gawith, and P. G. R. Smith, "Upconversion detection of 1.25 Gb/s mid-infrared telecommunications using a silicon avalanche photodiode," *Opt. Express, OE*, vol. 28, no. 23, pp. 34279–34289, Nov. 2020, doi: 10.1364/OE.404855.

[19] M. F. Witinski, J. B. Paul, and J. G. Anderson, "Pump-enhanced difference-frequency generation at 3.3 μm," *Appl. Opt., AO*, vol. 48, no. 13, pp. 2600–2606, May 2009, doi: 10.1364/AO.48.002600.

[20] K. Wang, X. Li, P. Wang, W. Hua, Z. Wang, and K. Han, "Broadband, Continuous-Wave, Mid-Infrared Generation Based on ASE Fiber Source," *Photonics*, vol. 9, no. 10, Art. no. 10, Oct. 2022, doi: 10.3390/photonics9100724.

[21] J. Mishra *et al.*, "Mid-infrared nonlinear optics in thin-film lithium niobate on sapphire," *Optica, OPTICA*, vol. 8, no. 6, pp. 921–924, Jun. 2021, doi: 10.1364/OPTICA.427428.

[22] C. Hu *et al.*, "High-efficient coupler for thin-film lithium niobate waveguide devices," *Opt. Express, OE*, vol. 29, no. 4, pp. 5397–5406, Feb. 2021, doi: 10.1364/OE.416492.

[23] L. Ledezma *et al.*, "Octave-spanning tunable infrared parametric oscillators in nanophotonics," *Science Advances*, vol. 9, no. 30, p. eadf9711, Jul. 2023, doi: 10.1126/sciadv.adf9711.

[24] A. Y. Hwang *et al.*, "Mid-infrared spectroscopy with a broadly tunable thin-film lithium niobate optical parametric oscillator." arXiv, Jul. 09, 2023. doi: 10.48550/arXiv.2307.04199.

[25] M. Santandrea, M. Stefszky, V. Ansari, and C. Silberhorn, "Fabrication limits of waveguides in nonlinear crystals and their impact on quantum optics applications," *New J. Phys.*, vol. 21, no. 3, p. 033038, Mar. 2019, doi: 10.1088/1367-2630/aaff13.

[26] N. I. Chunosov, "reZonator." Accessed: Jun. 06, 2023. [Online]. Available: http://rezonator.orion-project.org/

[27] "Detailed study of thermal lensing in Nd:YVO/sub 4/ under intense diode end-pumping." Accessed: Sep. 25, 2023. [Online]. Available: https://ieeexplore.ieee.org/document/947669/

[28] L. Flannigan, T. Kashak, and C.-Q. Xu, "Study of fundamental wave depletion in intracavity second harmonic generation," *Opt. Express, OE*, vol. 29, no. 5, pp. 6810–6823, Mar. 2021, doi: 10.1364/OE.417191.

[29] W. P. Risk, "Modeling of longitudinally pumped solid-state lasers exhibiting reabsorption losses," *J. Opt. Soc. Am. B, JOSAB*, vol. 5, no. 7, pp. 1412–1423, Jul. 1988, doi: 10.1364/JOSAB.5.001412.

[30] R. Boyd, *Nonlinear Optics*, 4th ed. Academic Press. Accessed: Sep. 26, 2023. [Online]. Available: https://shop.elsevier.com/books/nonlinear-optics/boyd/978-0-12-811002-7

[31] O. Gayer, Z. Sacks, E. Galun, and A. Arie, "Temperature and wavelength dependent refractive index equations for MgO-doped congruent and stoichiometric LiNbO3," *Appl. Phys. B*, vol. 91, no. 2, pp. 343–348, May 2008, doi: 10.1007/s00340-008-2998-2.

[32] Y. Bai, "Pumping wavelength related population inversion in Nd:doped laser," *AIP Advances*, vol. 10, no. 10, p. 105309, Oct. 2020, doi: 10.1063/5.0006436.

[33] L. Fornasiero, S. Kück, T. Jensen, G. Huber, and B. H. T. Chai, "Excited state absorption and stimulated emission of Nd3+ in crystals. Part 2: YVO4, GdVO4, and Sr5(PO4)3F," *Appl Phys B*, vol. 67, no. 5, pp. 549–553, Nov. 1998, doi: 10.1007/s003400050543.

[34] Y.-F. Chen and Y. P. Lan, "Comparison between c-cut and a-cut Nd:YVO4 lasers passively Q-switched with a Cr4+:YAG saturable absorber," *Appl Phys B*, vol. 74, no. 4, pp. 415–418, Apr. 2002, doi: 10.1007/s003400200814.

[35] T. W. Tukker, C. Otto, and J. Greve, "Elliptical-focusing effect on parametric oscillation and downconversion," *J. Opt. Soc. Am. B, JOSAB*, vol. 15, no. 9, pp. 2455–2461, Sep. 1998, doi: 10.1364/JOSAB.15.002455.

[36] S. Gagnon, B. Sylvestre, L. Gagnon, A. Koujelev, D. Gratton, and S. Hranilovic, "Recent developments in satellite laser communications: Canadian context," in *International Conference on Space Optical Systems and Applications (ICSOS)*, Corsica, France, Oct. 2012, pp. 1–8.